# Nonlocal Resonances in Pedestal High-Index-Contrast Metasurfaces based on a Silicon-on-Insulator Platform

P. Franceschini,[1,2] A. Tognazzi*,[2,3] G. Finco,[4] L. Carletti,[1,2] I. Alessandri,[1,2] A. C. Cino,[3] C. De Angelis,[1,2] O. Takayama,[5] R. Malureanu,[5] A. V. Lavrinenko,[5] and D. de Ceglia[1,2]

[1)] *Department of Information Engineering, University of Brescia, Via Branze 38, Brescia, 25123, Italy*

[2)] *National Institute of Optics - National Research Council (INO-CNR), Via Branze 45, Brescia, 25123, Italy*

[3)] *Department of Engineering, University of Palermo, Viale delle Scienze ed. 9, Palermo 90128, Italy*

[4)] *ETH Zurich, Department of Physics, Institute for Quantum Electronics, Optical Nanomaterial Group, Auguste-Piccard-Hof 1, 8093 Zurich, Switzerland.*

[5)] *Department of Electrical and Photonics Engineering, Technical University of Denmark, Ørsteds Plads, Building 345A, DK-2800 Kongens Lyngby, Denmark.*

(*Electronic mail: andrea.tognazzi@unipa.it)

(Dated:)

Subwavelength control of the electromagnetic field distribution represents one of the current challenges in photonics research. In this field, diffractive metasurfaces with spatially extended (*i.e.*, nonlocal) resonant modes have recently gained a great interest for their versatility in molding the electromagnetic field beyond the approximation of independent resonators. In this framework, we design an high-contrast nonlocal metasurface featuring modes situated in the third operating spectral window of optical communications. The optical properties of the fabricated metasurface are investigated by linear spectroscopy and numerical simulations. Our analysis allows to discern the magnetic and electric nature of the bounded modes by means of polarization-resolved reflectance measurements. Our results represent a step toward integrated nano-photonics in the telecom regime and open promising opportunities for the development of compact nonlinear optical devices.

In the last decades, the field of nano-photonics has witnessed a steady progress of small-footprint and high-performance optical devices with diverse functionalities for a wide variety of applications, from light manipulation to sensing[1–5]. This advancement has been fueled by the significant development and improvement of fabrication methods which are now capable to produce nano-structured materials with high precision. In this context, *metasurfaces* are emerging as a powerful tool to manipulate the properties of light, such as amplitude, phase, polarization and angular momentum, and to engineer light-matter interactions with a higher degree of versatility across the spectrum. Indeed, when considering light-matter interaction within objects with a size on the order of the impinging wavelength, structural modes are accessible and they provide a high field localization, which ultimately determines an enhancement of the performances[6–8], especially for nonlinear optical interactions such as frequency-mixing in which the intensity of nonlinearly scattered light scales superlinearly with the intensity of the input light[9]. Not only this aspect lead to the development of devices for dynamical light-modulation[10–16], but it is also crucial for the realization of nonlocal metasurfaces (NLM, *e.g.*, resonant gratings) for the efficient control of nonlinearly diffracted light[17–22]. Nonlocal metasurfaces have recently been proposed as promising candidates for sensing, since the propagation of an external light through guided mode resonances can be strongly modified under the exposure to a chemical specimen[23–27]. In particular, high-contrast NLMs (HC-NLMs) have gained increasing attention due to their enhanced ability to boost the optical field localization compared to conventional gratings, owing to the large index contrast between the diffractive elements of the grating and the low-index background material[28,29]. In this framework, silicon represents the most suitable constituent due to its high-refractive index, low-absorption losses in the near infrared region (NIR), high nonlinear coefficient, low-cost and mature nano-fabrication processes, and good compatibility with complementary metal-oxide-semiconductor (CMOS) technology[30–33]. Regarding sensing applications, an additional advantage of HC-NLM is the possibility to increase the area exposed to the analyte, thus improving the interaction with the environment, by the fabrication of pedestal HC-NLM, as recently demonstrated[29,34].

Previously, low refractive index substrate[35] and suspended metasurfaces[36] were employed in the mid infrared region to enhance electric field confinement. Here, we propose a Si-based pedestal HC-NLM featuring both bound-state-in-continuum[37,38] (BIC) modes and guided mode resonances (GMRs) at telecommunications wavelengths. First, we analyze the modes of the structure by numerically calculating the dispersion curves and the field distributions of the modes by using the finite element method (FEM). We then perform measurements of polarization-resolved spectra in the linear regime and compare them with spectra calculated numerically with the rigorous coupled-wave analysis (RCWA) under plane-wave excitation. Our results provide a scalable geometry for an efficient integration of HC-NLM in photonics devices which can be scaled down to telecommunication wavelengths.

The metasurface under study is a one-dimensional peri-

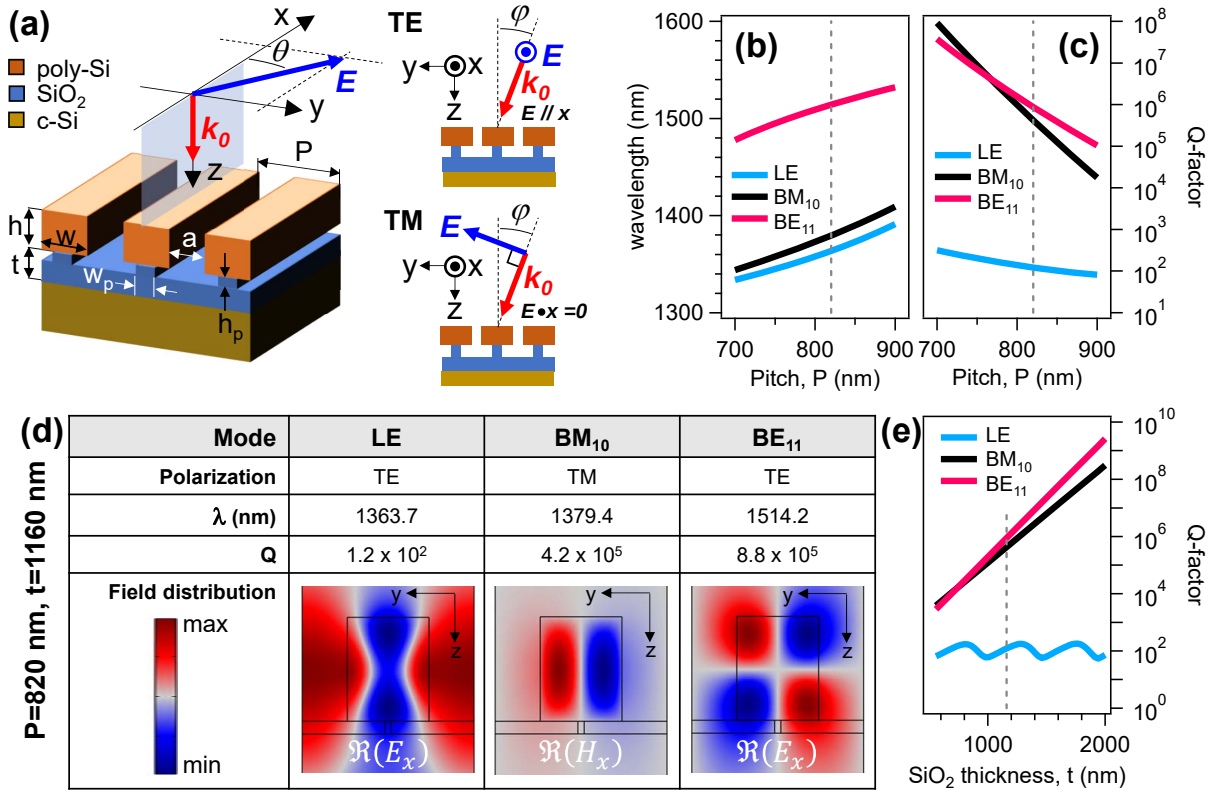


FIG. 1. **Metasurface Design.** (a) Sketch of the proposed metasurface. The Si bars, standing on top of $SiO_2$ pedestals of height $h_p$ and width $w_p$, have a width $w$ and a height $h$. Given a pitch $P$, the resulting slit aperture is $a = P - w$. The thickness of the $SiO_2$ layer is $t$. (b) Calculated dispersion curves of the eigen-wavelengths of modes in the NIR spectral region between 1300 and 1700-nm wavelength. (c) Calculated quality factor as a function of the pitch for LE, $BM_{10}$, and $BE_{11}$ modes. (d) Summary of the modes for $P = 820$ nm and for $t = 1160$ nm. The values of the spectral position (wavelength, $\lambda$) and quality factor ($Q$) of the modes are those at $\theta = 0°$. The insets show the spatial distribution of the field component along the $x$-axis (electric and induction field, $E$ and $H$, respectively). In the colorscale, blue (red) color corresponds to negative (positive) values. (e) Calculated quality factor as a function of the $SiO_2$ layer thickness for LE, $BM_{10}$, and $BE_{11}$ modes. LE: leaky; $BM_{10}$: bounded magnetic with mode shape 1 ($y$-axis), 0 ($z$-axis); $BE_{11}$: bounded electric with mode shape 1 ($y$-axis), 1 ($z$-axis). The gray vertical dotted lines indicate the value of the parameter of the fabricated metasurface.

odic structure (along the $y$ direction), as sketched in Fig. 1(a). The unit cell includes a bar with rectangular cross section (width $w$ and height $h$), with its long axis aligned to the $x$-direction, sitting on top of a pedestal with height $h_p$ and width $w_p = w - 2h_p$. The latter structural element helps keeping the bar suspended, so that, by a suitable choice of materials, this further enhances the index contrast between the groove and the surrounding environment. From a fabrication point of view, etching represents a reliable technique to achieve this configuration, as recently demonstrated[34]. As shown in Fig. 1(a), in the proposed metasurface, we adopted silicon (Si) as the constitutive material for the bar and silica ($SiO_2$) for the pedestal and the uppermost layer of the substrate [with total thickness $t$, as shown in Fig. 1(a)].

To obtain a photonic structure supporting resonant modes in the third operating window of optical communication ($\sim$ 1500 nm), we properly designed the geometrical parameters of the metasurface. In particular, given its geometry, the proposed structure may support both optical BIC and guided (or leaky) modes. The latter type of modes, appearing as sharp resonances in spectra (GMRs), are modes propagating along the grating periodicity axis ($y$-axis) and occurs when the following phase-matching condition is fulfilled[39]:

$$k_{\mathrm{GMR}} \simeq |k_0 \sin(\varphi) + 2\pi m/P|, \qquad m = \pm(1,2,3,\ldots), \quad (1)$$

where $k_{\mathrm{GMR}}$ is the wavevector of the guided mode, $k_0 = 2\pi/\lambda_0$ is the wavenumber of the impinging light at wavelength $\lambda_0$ (in vacuum) and $\varphi$ is the angle of incidence with respect to the normal to the surface [see Fig. 1(a)]. Therefore, a modal analysis was performed with FEM simulations (Comsol Multiphysics) to reveal the presence of modes spectrally located in the NIR. In our design approach, we focused on the dependence of the modes on two geometrical parameters: the grating pitch and the $SiO_2$ layer thickness and the results are shown in Fig. 1(b)-(e). As suggested by Fig. 1(b), which displays the dispersion curves as a function of the grating pitch, the structure supports three modes in the 1300-1600-nm wavelength range: an electric BIC-type mode $\sim$ 1500 nm (magenta curve), labelled $BE_{11}$, a magnetic BIC-type mode, labelled $BM_{11}$, and an electric leaky mode, labelled LE in the range 1330-1410 nm. BIC-type modes are characterized by odd symmetry of their eigenfields [see Fig. 1(d)]. As expected, the

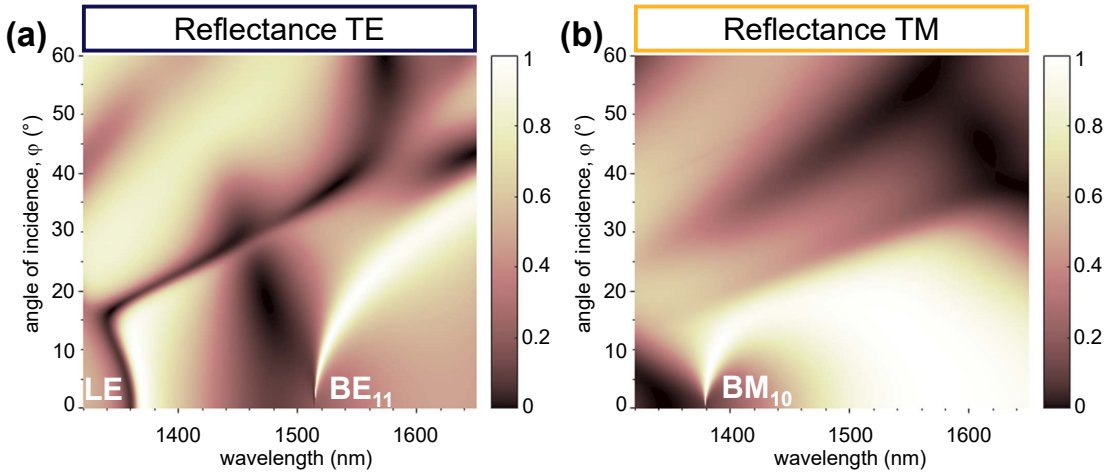


FIG. 2. **Angle-Resolved Reflectance spectra.** Simulated reflectance of the HC-NLM as a function of wavelength and angle of incidence for TE (a) and TM (b) polarization.

mode eigenwavelength increases with increasing pitch with a shallow dependence. On the other hand, as depicted in Fig. 1(c), the pitch dependence of the $Q$-factor exhibits a shallow decrease in the case of the LE mode (blue curve) and an exponential drop for the BIC-type modes $BM_{10}$ and $BE_{11}$ (black and magenta curve, respectively). This different behavior is ruled by diffraction, as detailed in the supplementary material, and it is related to the nature of the modes supported by the metasurface. In theory, BIC are characterized by an infinite $Q$-factor. However, in experimental conditions, they can appear as resonances with finite $Q$ due to different kinds of radiation leakage, including tilting of sidewall of Si grating bars, finite number of periods, finite size of the source, and opening of higher-order diffraction channels. In the structure under investigation, while the $0^{th}$ diffraction order may be forbidden by symmetry protection for modes having eigenfields with odd parity, light emission into higher orders of diffraction is possible under proper conditions. Higher-order diffraction into the silicon substrate limits the $Q$ factor of symmetry-protected BICs. In addition, the amount of diffraction leakage significantly depends on the grating pitch, as illustrated in Fig. 1(c). A diffraction channel is opened when the diffraction limit is exceeded, *i.e.*, $P \cdot n_{sub} > \lambda_\Gamma$, where $n_{sub}$ is the refractive index of the substrate and $\lambda_\Gamma$ is the mode central wavelength at the $\Gamma$ point. In the case of $BM_{10}$ and $BE_{11}$ modes, centered at $\lambda_\Gamma^{BM10}$ and $\lambda_\Gamma^{BE11}$, we obtain $P \cdot n_{Si} > \lambda_\Gamma^{BE11} > \lambda_\Gamma^{BM10}$, for $P$ in the range 700-900 nm. The eigenfields of these two modes are evanescent in the $SiO_2$ region while they are propagative in the Si substrate due to higher-order diffraction. The *evanescent-wave coupling* between the BIC and the substrate, which is critically dependent on the thickness of $SiO_2$ was first reported in Ref.[40], where the dependence of the $Q$-factor on the oxide layer thickness was studied. The role of the $SiO_2$ layer thickness is highlighted in Fig. 1(e), which shows an exponential increase of the $Q$ factor with the silicon dioxide thickness that is consistent with the results reported in Ref.[40]. In addition to the previous study (focusing on BIC modes turning into resonant states due to the high-index substrate), we also study a GMR with leakage occurring at $0^{th}$ diffraction order. In particular, we note an oscillating modulation of the $Q$-factor of the LE mode as a function of $t$ [blue curve in Fig. 1(e)]. This behavior is due to the fact that, in contrast to the case of the BIC-type modes, the LE mode does leak radiation in the normal direction in the $SiO_2$ region, and this radiation may be reflected back towards the grating by the interface with Si, hence generating an interference effect that is regulated by $t$. The result of this interference is the Fabry-Pérot-like oscillation of the $Q$ factor. The modal analysis underlines the strong dependence of the $Q$-factor on the grating pitch. Therefore, given the shallower dependence of the central wavelength on the same parameter, the pitch represents an effective tuning parameter for the design of this kind of metasurfaces. So, in order to ensure both the proper matching with respect to fabrication tolerances and a high $Q$-factor for the $BE_{11}$ mode occurring in the third operating window of optical communications, the value $P = 820$ nm was chosen together with $t = 1160$ nm. Additionally, the modal analysis allows to unveil the polarization excitation condition of each mode. The LE eigenmode, featuring an even parity along the $y$-axis [Fig. 1(d)], can be excited by an electric field with TE (Transverse Electric) polarization, *i.e.*, $\mathbf{E} \parallel x$ [$\theta = 0$, Fig. 1(a)]. Regarding the BIC-type eigenmodes, while $BM_{10}$ mode exhibits an odd parity only along the $y$-axis, $BE_{11}$ mode shows an additional parity also in the $z$ direction. In view of the nature of the polarization of the external excitation, TM [Transverse Magnetic, $\mathbf{E} \cdot x = 0$, Fig. 1(a)] and TE are required for exciting $BM_{10}$ and $BE_{11}$ modes, respectively.

The polarization-angle-resolved reflectivity spectra of the HC-NLM provide additional information about the three resonances. In Fig. 2 we show the reflectance, calculated by the RCWA model (see supplementary material for more details), as a function of the incident angle $\varphi$ and the wavelength $\lambda$, for TE [$\theta = 0°$, panel (a)] and TM [$\theta = 90°$, panel (b)] polarizations. Interestingly, for TE mode, two sharp features can be seen at $\lambda \sim 1360$ nm (LE) and $\lambda \sim 1515$ nm ($BE_{11}$), both for $\varphi \sim 0°$; while, for TM mode, a sharp feature appears at

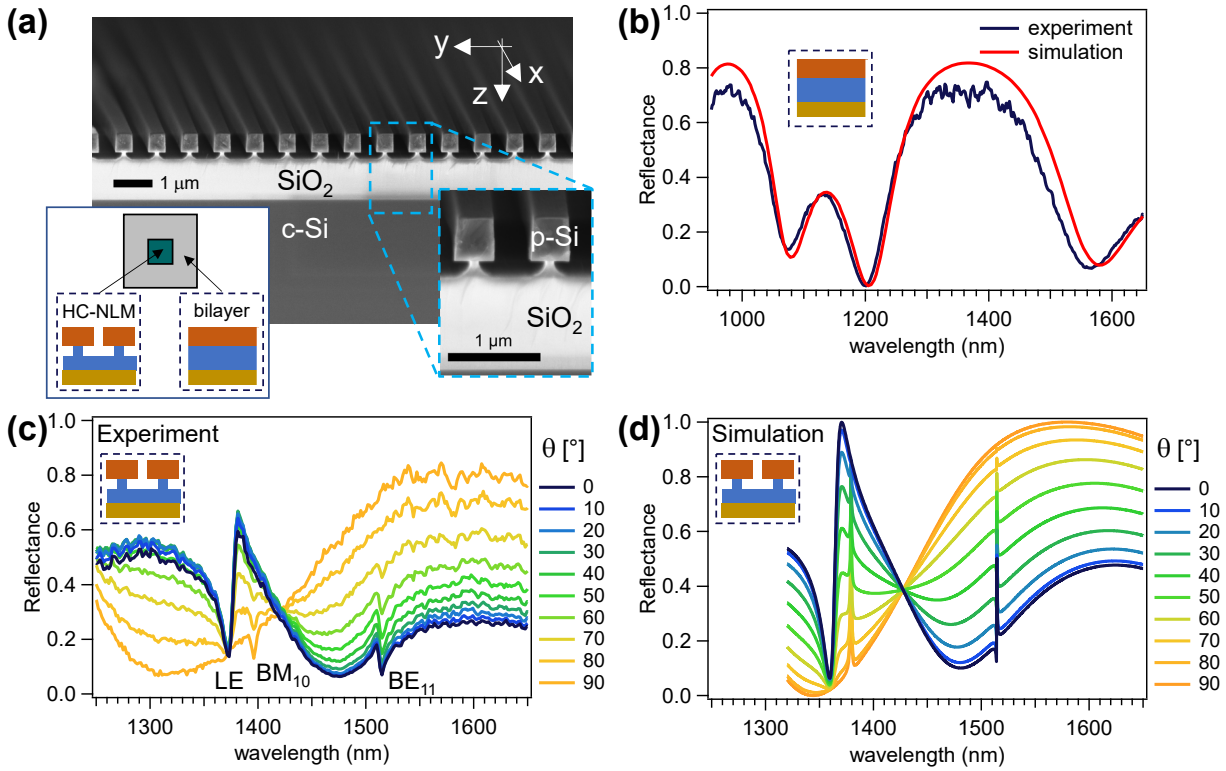


FIG. 3. **Structural and Optical Chacterization.** (a) SEM image of the fabricated metasurface. Parameters of the structure. $P = 820$ nm; $h_p = 160$ nm; $w_p = 73$ nm; $w = 393$ nm; $h = 500$ nm; $a = 427$ nm. Inset: top view of the sample. The central (surrounding) region corresponds to the HC-NLM (the Si/$SiO_2$/Si bilayer). (b) Reflectance spectrum of the bilayer region: experimental (dark blue) and simulated (red). (c) Experimental and (d) simulated reflectance spectra of the HC-NLM at various values of the polarization angle. The dashed frames display a cross-sectional view of the structure under analysis.

$\lambda \sim 1380$ nm ($BM_{10}$), for $\varphi \sim 0°$. Moreover, we note that both $BM_{10}$ and $BE_{11}$ spectral features disappear at $\varphi = 0°$; while, on the contrary, the spectral feature of LE mode is clearly visible at normal incidence (*i.e.*, $\varphi = 0°$). These details confirm that LE is a leaky mode regardless of $\varphi$, but highlight also the leaky behaviour of $BM_{10}$ and $BE_{11}$ modes for $\varphi > 0°$. The former is consistent with their bound nature associated with symmetry protection at $\varphi = 0°$, as discussed in the previous section.

We detail the fabrication of the designed HC-NLM in the supplementary material. We adopt Scanning electron microscopy (SEM) to investigate the quality of the fabricated HC-NLM structure and we report in Fig. 3(a) a cross sectional view which corresponds to the central region (5 mm × 5 mm) of the whole sample [see inset in Fig. 3(a)]. We employ an home-built spectroscopy apparatus for linear reflectivity measurements to optically characterize the fabricated metasurface (see supplementary material for more details). First, we investigate the spectral properties of the bilayer region. Fig. 3(b) reports the reflectance curve in the NIR spectral region (950 − 1650 nm) at normal incidence. The spectrum is characterized by broadband peaks, whose nature has been investigated through a theoretical model based on RCWA method[41]. As input parameters for the model, the layer thickness values obtained from SEM were adopted (i.e., $h = 500$ nm and $t = 1160$ nm, see Fig. 3). Moreover, the optical properties (refractive index) of poly-Si were obtained from ellipsometry measurements, while those of $SiO_2$ and c-Si from Ref.[42] and Ref.[43] , respectively. The model [red curve in Fig. 3(b)] well reproduces the experimental data. In particular, the minima in the calculated spectrum originate from Fabry-Pérot modes and their spectral position matches with the minima in the experimental data. The good agreement between the experimental data and the model highlights the quality of the fabrication process and allows to validate the capability of the setup.

Now, we turn our attention to the HC-NLM. It is useful to remind that, in our reference frame, the $x$-axis is the direction parallel to the bars and the $z$-axis corresponds to the normal to the sample surface [see Fig. 1(a)]. Moreover, $yz$ is the plane of incidence; therefore, $\mathbf{k}_0 = 2\pi n_0/\lambda\ (\sin\varphi\,\hat{y} + \cos\varphi\,\hat{z})$. Reflectance spectra (at normal incidence) of the HC-NLM were measured for polarization directions of the **E** field varying from TE ($\theta = 0°$) to TM ($\theta = 90°$) mode and the results are displayed in Fig. 3(c). The spectra of the metasurface are characterized by broadband background resonances (located at $\sim 1300$ nm and $\sim 1600$ nm), whose amplitude varies as a function of the polarization angle $\theta$. Interestingly, three narrower features appear, whose spectral position well matches that predicted in the design model. Therefore, the peaks in the reflectance spectra are ascribed to LE ($\sim 1370$ nm), $BM_{10}$

TABLE I. Summary of the parameters retrieved from fitting a Fano lineshape to the experimental reflectance spectra.

| Mode | $\theta$ (°) | $\lambda_r$ (nm) | $\Delta\lambda$ (nm) | $q$ |
|---|---|---|---|---|
| LE | 0 | $1377.4 \pm 0.2$ | $9.9 \pm 0.2$ | $-0.98 \pm 0.03$ |
| $BM_{10}$ | 90 | $1395.4 \pm 0.3$ | $4.1 \pm 0.2$ | $0.22 \pm 0.06$ |
| $BE_{11}$ | 0 | $1513.3 \pm 0.2$ | $3.7 \pm 0.1$ | $0.57 \pm 0.05$ |

($\sim$ 1400 nm), and $BE_{11}$ ($\sim$ 1515 nm) modes. In particular, we underline that the resonances LE and $BE_{11}$ disappear when $\theta$ increases (*i.e.*, moving from the TE to the TM mode), while resonance $BM_{10}$ shows an opposite behaviour. In order to better understand the nature of these spectral features, RCWA simulations were performed to calculate reflectance spectra under plane-wave illumination. The reflectance spectra, obtained by considering a numerical aperture NA$= 0.03$ (*i.e.*, averaging over values of $\varphi$ ranging from 0 to $\sim 2^\circ$), are in good agreement with the experimental data [see Fig. 3(d)]. This result confirms that the experimental probe light includes a small fraction of off-normal wavevector components $\mathbf{k}_0 \cdot \hat{y} \neq 0$ associated with the non-zero numerical aperture. Therefore, this further analysis unveils that the three narrow peaks in the reflectance spectra are the signature, in the form of Fano resonances, of the interference between the continuum of modes of the incident light and the discrete spectrum related to the leaky component of LE, $BM_{10}$, and $BE_{11}$ modes[44]. A Fano lineshape[45] has been fitted to the experimental curves in order to retrieve spectral position ($\lambda_r$), bandwidth ($\Delta\lambda$), and profile index ($q$) of the three resonances (see supplementary material for more details). The results are summarized in Tab. I. We note a difference between the experimental and calculated profile of the resonances. Our analysis, outlined in the supplementary material, indicates that the differences between experimental and calculated profile of resonances are due to: (i) the non-ideal response of the polarizer, (ii) the limited spectral and angular resolution of the setup, and (iii) fabrication imperfections, especially related to the pedestal thickness.

We theoretically investigated and experimentally demonstrated a Si-based HC-NLM supporting BIC modes in the third window of the telecom spectrum. Our results show that introducing a low refractive index pedestal structure supporting a high-index grating leads to the production of high-quality HC-NLMs. We performed polarization resolved reflectivity measurements and compared the results with RCWA and FEM simulations to unveil the electric and magnetic nature of BIC modes. Simulations and experiments show good agreement, confirming the high quality of the fabricated samples. Our results set HC-NLM as a promising technology for integrated nanophotonics for telecommunications, and for the development of compact sensors and nonlinear optical devices.

See the supplementary material for more details on sample fabrication, spectroscopy setup, rigorous coupled-wave analysis, and analysis of the experimental reflectance spectra.

A. Tognazzi acknowledges the financial support from the European Union through "FESR o FSE, PON Ricerca e Innovazione 2014-2020 - DM 1062/2021" and the University of Palermo through "Fondo Finalizzato alla Ricerca di Ateneo 2023 (FFR2023)". O. Takayama acknowledges the financial support from the Independent Research Fund Denmark (DFF), Denmark, Research Project 2, "No. 8022-00387B." The authors acknowledge the financial support from the European Community through the “METAFAST” project (H2020-FETOPEN-2018-2020, grant agreement no. 899673) and Ministero Italiano dell’Istruzione (MIUR) through the "METEOR" project (PRIN-2020, 2020EY2LJT_002).

## AUTHOR DECLARATIONS

### Conflict of Interest

The authors have no conflicts to disclose.

### Author Contributions

**P. Franceschini**. Data curation (equal); Formal analysis (equal); Investigation (equal); Software (equal); Writing – original draft (equal); Writing – review & editing (equal). **A. Tognazzi**. Data curation (equal); Funding acquisition (equal); Investigation (equal); Writing – original draft (equal); Writing – review & editing (equal). **G. Finco**. Conceptualization (lead); Data curation (equal); Formal analysis (equal); Investigation (equal); Resources (equal); Software (equal); Validation (equal); Writing – original draft (equal); Writing – review & editing (equal). **L. Carletti**. Data curation (equal); Investigation (equal); Writing – review & editing (equal). **I. Alessandri**. Investigation (equal); Resources (equal); Writing – review & editing (equal). **A. C. Cino**. Writing – review & editing (equal). **C. De Angelis**. Funding acquisition (equal); Writing – review & editing (equal). **O. Takayama**. Data curation (equal); Funding acquisition (equal); Resources (equal); Writing – review & editing (equal). **R. Malureanu**. Data curation (equal); Resources (equal); Writing – review & editing (equal). **A. V. Lavrinenko**. Conceptualization (equal); Resources (equal); Writing – review & editing (equal). **D. de Ceglia**. Conceptualization (equal); Formal analysis (equal); Methodology (leading); Project Administration (leading); Software (equal); Validation (equal); Writing – original draft (supporting); Writing – review & editing (equal).

## DATA AVAILABILITY

The data that supports the findings of this study are available within the article and its supplementary material.

## REFERENCES


[1] Z.-J. Yang, R. Jiang, X. Zhuo, Y.-M. Xie, J. Wang, and H.-Q. Lin, "Dielectric nanoresonators for light manipulation," Physics Reports **701**, 1–50 (2017).

[2] A. C. Overvig, S. Shrestha, S. C. Malek, M. Lu, A. Stein, C. Zheng, and N. Yu, "Dielectric metasurfaces for complete and independent control of the optical amplitude and phase," Light: Science & Applications **8** (2019), 10.1038/s41377-019-0201-7.

[3] R. Paniagua-Domínguez, B. Luk'yanchuk, A. Miroshnichenko, and J. A. Sánchez-Gil, "Dielectric nanoresonators and metamaterials," Journal of Applied Physics **126**, 150401 (2019).

[4] C. Li, P. Yu, Y. Huang, Q. Zhou, J. Wu, Z. Li, X. Tong, Q. Wen, H.-C. Kuo, and Z. M. Wang, "Dielectric metasurfaces: From wavefront shaping to quantum platforms," Progress in Surface Science **95**, 100584 (2020).

[5] H. Altug, S.-H. Oh, S. A. Maier, and J. Homola, "Advances and applications of nanophotonic biosensors," Nature Nanotechnology **17**, 5–16 (2022).

[6] M. V. Rybin, K. L. Koshelev, Z. F. Sadrieva, K. B. Samusev, A. A. Bogdanov, M. F. Limonov, and Y. S. Kivshar, "High-$q$ supercavity modes in subwavelength dielectric resonators," Physical Review Letters **119**, 243901 (2017).

[7] J. Yang and J. A. Fan, "Analysis of material selection on dielectric metasurface performance," Optics Express **25**, 23899 (2017).

[8] S. M. Kamali, E. Arbabi, A. Arbabi, and A. Faraon, "A review of dielectric optical metasurfaces for wavefront control," Nanophotonics **7**, 1041–1068 (2018).

[9] L. Carletti, K. Koshelev, C. De Angelis, and Y. Kivshar, "Giant nonlinear response at the nanoscale driven by bound states in the continuum," Phys. Rev. Lett. **121**, 033903 (2018).

[10] M. Sun, X. Xu, X. W. Sun, X. Liang, V. Valuckas, Y. Zheng, R. Paniagua-Domínguez, and A. I. Kuznetsov, "Efficient visible light modulation based on electrically tunable all dielectric metasurfaces embedded in thin-layer nematic liquid crystals," Scientific Reports **9** (2019), 10.1038/s41598-019-45091-5.

[11] Y. Che, X. Wang, Q. Song, Y. Zhu, and S. Xiao, "Tunable optical metasurfaces enabled by multiple modulation mechanisms," Nanophotonics **9**, 4407–4431 (2020).

[12] S. C. Malek, A. C. Overvig, S. Shrestha, and N. Yu, "Active nonlocal metasurfaces," Nanophotonics **10**, 655–665 (2020).

[13] S. Abdollahramezani, O. Hemmatyar, M. Taghinejad, H. Taghinejad, Y. Kiarashinejad, M. Zandehshahvar, T. Fan, S. Deshmukh, A. A. Eftekhar, W. Cai, E. Pop, M. A. El-Sayed, and A. Adibi, "Dynamic hybrid metasurfaces," Nano Letters **21**, 1238–1245 (2021).

[14] B. Li, R. Camacho-Morales, N. Li, A. Tognazzi, M. Gandolfi, D. de Ceglia, C. De Angelis, A. A. Sukhorukov, and D. N. Neshev, "Fundamental limits for transmission modulation in $VO_2$ metasurfaces," Photonics Research **11**, B40 (2022).

[15] D. Zhang, Y. Chen, S. Gong, W. Wu, W. Cai, M. Ren, X. Ren, S. Zhang, G. Guo, and J. Xu, "All-optical modulation of quantum states by nonlinear metasurface," Light: Science & Applications **11** (2022), 10.1038/s41377-022-00744-5.

[16] P. P. Iyer, N. Karl, S. Addamane, S. D. Gennaro, M. B. Sinclair, and I. Brener, "Sub-picosecond steering of ultrafast incoherent emission from semiconductor metasurfaces," Nature Photonics (2023), 10.1038/s41566-023-01172-6.

[17] L. Wang, S. Kruk, K. Koshelev, I. Kravchenko, B. Luther-Davies, and Y. Kivshar, "Nonlinear wavefront control with all-dielectric metasurfaces," Nano Letters **18**, 3978–3984 (2018).

[18] L. Carletti, M. Gandolfi, D. Rocco, A. Tognazzi, D. de Ceglia, M. A. Vincenti, and C. De Angelis, "Reconfigurable nonlinear response of dielectric and semiconductor metasurfaces," Nanophotonics **10**, 4209–4221 (2021).

[19] N. Mao, Y. Tang, M. Jin, G. Zhang, Y. Li, X. Zhang, Z. Hu, W. Tang, Y. Chen, X. Liu, K. Li, K. Cheah, and G. Li, "Nonlinear wavefront engineering with metasurface decorated quartz crystal," Nanophotonics **11**, 797–803 (2021).

[20] L. Carletti, A. Zilli, F. Moia, A. Toma, M. Finazzi, C. De Angelis, D. N. Neshev, and M. Celebrano, "Steering and encoding the polarization of the second harmonic in the visible with a monolithic $LiNbO_3$ metasurface," ACS Photonics **8**, 731–737 (2021).

[21] K. I. Okhlopkov, A. Zilli, A. Tognazzi, D. Rocco, L. Fagiani, E. Mafakheri, M. Bollani, M. Finazzi, M. Celebrano, M. R. Shcherbakov, C. De Angelis, and A. A. Fedyanin, "Tailoring third-harmonic diffraction efficiency by hybrid modes in high-q metasurfaces," Nano Letters **21**, 10438–10445 (2021).

[22] A. Tognazzi, K. I. Okhlopkov, A. Zilli, D. Rocco, L. Fagiani, E. Mafakheri, M. Bollani, M. Finazzi, M. Celebrano, M. R. Shcherbakov, A. A. Fedyanin, and C. De Angelis, "Third-harmonic light polarization control in magnetically resonant silicon metasurfaces," Optics Express **29**, 11605 (2021).

[23] D. Tanasković, M. Obradov, O. Jakšić, and Z. Jakšić, "Nonlocal effects in double fishnet metasurfaces nanostructured at deep subwavelength level as a path toward simultaneous sensing of multiple chemical analytes," Photonics and Nanostructures - Fundamentals and Applications **18**, 36–42 (2016).

[24] S. Zhang, C. L. Wong, S. Zeng, R. Bi, K. Tai, K. Dholakia, and M. Olivo, "Metasurfaces for biomedical applications: imaging and sensing from a nanophotonics perspective," Nanophotonics **10**, 259–293 (2020).

[25] B. I. Karawdeniya, A. M. Damry, K. Murugappan, S. Manjunath, Y. M. N. D. Y. Bandara, C. J. Jackson, A. Tricoli, and D. Neshev, "Surface functionalization and texturing of optical metasurfaces for sensing applications," Chemical Reviews **122**, 14990–15030 (2022).

[26] J. Qin, S. Jiang, Z. Wang, X. Cheng, B. Li, Y. Shi, D. P. Tsai, A. Q. Liu, W. Huang, and W. Zhu, "Metasurface micro/nano-optical sensors: Principles and applications," ACS Nano **16**, 11598–11618 (2022).

[27] Y. H. Ko, K. J. Lee, F. A. Simlan, and R. Magnusson, "Singular states of resonant nanophotonic lattices," Nanophotonics **12**, 263–272 (2023).

[28] C. J. Chang-Hasnain and W. Yang, "High-contrast gratings for integrated optoelectronics," Adv. Opt. Photon. **4**, 379–440 (2012).

[29] G. Finco, M. Z. Bideskan, L. Vertchenko, L. Y. Beliaev, R. Malureanu, L. R. Lindvold, O. Takayama, P. E. Andersen, and A. V. Lavrinenko, "Guided-mode resonance on pedestal and half-buried high-contrast gratings for biosensing applications," Nanophotonics **10**, 4289–4296 (2021).

[30] T. P. Sidiki and C. M. S. Torres, "Silicon-based nanostructures," in *Nanostructured Materials and Nanotechnology* (Elsevier, 2002) pp. 387–443.

[31] S. V. Makarov, A. S. Zalogina, M. Tajik, D. A. Zuev, M. V. Rybin, A. A. Kuchmizhak, S. Juodkazis, and Y. Kivshar, "Light-induced tuning and reconfiguration of nanophotonic structures," Laser & Photonics Reviews **11**, 1700108 (2017).

[32] I. Staude and J. Schilling, "Metamaterial-inspired silicon nanophotonics," Nature Photonics **11**, 274–284 (2017).

[33] Z. Zhou, J. Li, R. Su, B. Yao, H. Fang, K. Li, L. Zhou, J. Liu, D. Stellinga, C. P. Reardon, T. F. Krauss, and X. Wang, "Efficient silicon metasurfaces for visible light," ACS Photonics **4**, 544–551 (2017).

[34] L. Y. Beliaev, P. G. Stounbjerg, G. Finco, A.-I. Bunea, R. Malureanu, L. R. Lindvold, O. Takayama, P. E. Andersen, and A. V. Lavrinenko, "Pedestal high-contrast gratings for biosensing," Nanomaterials **12**, 1748 (2022).

[35] A. S. L. Krishna, S. Menon, A. Prosad, and V. Raghunathan, "Mid-infrared quasi-BIC resonances with sub-wavelength slot mode profiles in germanium-based coupled guided-mode resonance structures," Photonics Research **10**, 68 (2021).

[36] J. M. Foley, S. M. Young, and J. D. Phillips, "Symmetry-protected mode coupling near normal incidence for narrow-band transmission filtering in a dielectric grating," Physical Review B **89**, 165111 (2014).

[37] D. C. Marinica, A. G. Borisov, and S. V. Shabanov, "Bound states in the continuum in photonics," Physical Review Letters **100**, 183902 (2008).

[38] S. Joseph, S. Pandey, S. Sarkar, and J. Joseph, "Bound states in the continuum in resonant nanostructures: an overview of engineered materials for tailored applications," Nanophotonics **10**, 4175–4207 (2021).

[39] G. Y. Wang, S. D. Koehler, and E. M. Garmire, "Quasi-phase-matched second-harmonic generation from femtosecond pulses in chirped gratings," in *OSA Annual Meeting* (Optica Publishing Group, 1993).

[40] Z. F. Sadrieva, I. S. Sinev, K. L. Koshelev, A. Samusev, I. V. Iorsh, O. Takayama, R. Malureanu, A. A. Bogdanov, and A. V. Lavrinenko, "Transition from optical bound states in the continuum to leaky resonances: Role of substrate and roughness," ACS Photonics **4**, 723–727 (2017).

[41] M. G. Moharam, T. K. Gaylord, E. B. Grann, and D. A. Pommet, "Formulation for stable and efficient implementation of the rigorous coupled-wave analysis of binary gratings," Journal of the Optical Society of America A **12**, 1068 (1995).

[42]I. H. Malitson, "Interspecimen comparison of the refractive index of fused silica∗,†," J. Opt. Soc. Am. **55**, 1205–1209 (1965).
[43]C. D. Salzberg and J. J. Villa, "Infrared refractive indexes of silicon germanium and modified selenium glass∗," J. Opt. Soc. Am. **47**, 244–246 (1957).
[44]M. F. Limonov, M. V. Rybin, A. N. Poddubny, and Y. S. Kivshar, "Fano resonances in photonics," Nature Photonics **11**, 543–554 (2017).
[45]U. Fano, "Effects of configuration interaction on intensities and phase shifts," Physical Review **124**, 1866–1878 (1961).
[46]D. de Ceglia, G. D'Aguanno, N. Mattiucci, M. A. Vincenti, and M. Scalora, "Enhanced second-harmonic generation from resonant GaAs gratings," Opt. Lett. **36**, 704–706 (2011).
[47]B. Chang, P. Leussink, F. Jensen, J. Hübner, and H. Jansen, "DREM: Infinite etch selectivity and optimized scallop size distribution with conventional photoresists in an adapted multiplexed bosch DRIE process," Microelectronic Engineering **191**, 77–83 (2018).